

A COMBINED *CHANDRA* AND LAMOST STUDY OF STELLAR ACTIVITYLIN HE^{1,2}, SONG WANG², JIFENG LIU^{2,3}, ROBERTO SORIA^{3,4,5}, ZHONGRUI BAI², HUIQIN YANG^{2,3}, YU BAI², JINCHENG GUO⁶*Draft version December 17, 2018*

ABSTRACT

We probed stellar X-ray activity over a wide range of stellar parameters, using *Chandra* and LAMOST data. We measured the X-ray-to-bolometric luminosity ratio ($R_X = L_X/L_{\text{bol}}$) for 484 main-sequence stars, and found a bimodal distribution for G and K types. We interpret this bimodality as evidence of two sub-populations with different coronal temperatures, which are caused by different coronal heating rates. Using the metallicity and velocity information, we find both of the two sub-populations are mostly located in the thin disk. We find no trend of R_X with stellar age for stars older than ~ 4 Gyr; there is a trough in the R_X vs age distribution, with the lowest range of R_X appearing at ages around 2 Gyr. We then examined the correlation between R_X and $R_{\text{H}\alpha}$ (proxy of chromospheric activity): we find that the two quantities are well correlated, as found in many earlier studies. Finally, we selected a sample of twelve stars with X-ray flares, and studied the light-curve morphology of the flares. The variety of flare profiles and timescales observed in our sample suggests the contribution of different processes of energy release.

Keywords: X-rays: stars – stars: activity – stars: late-type

1. INTRODUCTION

Stellar activity has been extensively explored in the X-ray regime for nearly forty years (Vaiana et al. 1981; Schmitt et al. 1985; Rosner et al. 1985). From the *Einstein* mission, X-ray observations have shown that X-ray emission is prevalent among almost all stellar classes (e.g., Stocke et al. 1983; Maccacaro et al. 1988; Stocke et al. 1991), although with different mechanisms for early and late-type stars (see Narain & Ulmschneider 1990; Güdel 2004, for a review). In general, the hottest and most massive stars emit X-rays arising from either small-scale shocks in their winds or collisions between the wind and circumstellar material (Lucy & White 1980; Parkin et al. 2009), while X-ray emission from late-type stars is attributed to the presence of a magnetic corona (Vaiana et al. 1981). Previous studies have made significant progress, both observationally and theoretically, in understanding the correlation between corona and magnetic fields (e.g., Klimchuk 2006; Cranmer et al. 2007). However, some detailed physical processes, such as coronal heating, are still poorly understood, and remain open issues in current astrophysics.

The study of stellar activity is important because it can provide new constraints for magnetic dynamo models. A number of proxies have been used to study the activity of different stellar components, such as the corona (X-ray emission), the chromosphere (Ca II HK;

Mg II; H α ; optical flares; NUV flux), the transition region (FUV flux), and the photosphere (star spots). Observations have revealed empirical scalings of these proxies, and therefore of magnetic activity, with rotation period or Rossby number, the latter of which is a ratio of rotation period to convective turnover time (e.g., Pallavicini et al. 1981; Vilhu 1984; Micela et al. 1985; Pizzolato et al. 2003; Wright et al. 2011; Gondoin 2012; Mathur et al. 2014; Blackman & Thomas 2015). It is believed that the generation of magnetic energy by large-scale dynamo action is driven by rotation and convection (Charbonneau 2010; Reiners et al. 2014). In the solar-type dynamo mechanism ($\alpha\Omega$ dynamo), the magnetic field is generated in the deep convection zones due to the interior radial differential rotation; the magnetic field then rises to the photosphere and produces chromospheric heating through the interaction with the uppermost convection zones (e.g., Cardini & Cassatella 2007; Cincunegui et al. 2007).

In parallel with the uncertainty on the physical heating processes, the magnetic activity evolution also remains unclear. Although many authors have investigated the dependence of chromospheric and coronal emission levels on the stellar age and evolutionary stage, the results are still under debate and improved (Pizzolato et al. 2003; Lyra & Porto de Mello 2005; Pace 2013; Zhao et al. 2013; Booth et al. 2017). In general, stellar activity and rotation are observed to decay with stellar age (Wilson 1963; Kraft 1967; Skumanich 1972; Simon et al. 1985; Pace & Pasquini 2004; Cardini & Cassatella 2007; Mamajek & Hillenbrand 2008). Furthermore, the coronal and chromospheric emission have been used as age indicators (Soderblom et al. 1991; Donahue 1993; Lachaume et al. 1999; Mamajek & Hillenbrand 2008; Soderblom 2010; Jeffries 2014). However, the age-activity relation constructed from X-ray emission is quite uncertain, since the X-ray flux is significantly variable (Soderblom 2010). More effort is needed to better understand the activity evolution and to improve the age-

¹ School of Astronomy and Space Science and Key Laboratory of Modern Astronomy and Astrophysics, Nanjing University, Nanjing, 210093, P. R. China

² Key Laboratory of Optical Astronomy, National Astronomical Observatories, Chinese Academy of Sciences, Beijing 100101, China; songw@bao.ac.cn

³ College of Astronomy and Space Sciences, University of Chinese Academy of Sciences, Beijing 100049, China

⁴ International Centre for Radio Astronomy Research, Curtin University, GPO Box U1987, Perth, WA 6845, Australia

⁵ Sydney Institute for Astronomy, School of Physics A28, The University of Sydney, Sydney, NSW 2006, Australia

⁶ Department of Astronomy, Peking University, Beijing 100871, China

activity relation as a dating technique.

A large sample of late-type stars with known stellar parameters is well suitable to investigate stellar activity and to explore the correlation between stellar activity and other stellar properties. These are helpful for understanding coronal heating processes, as well as the evolution of stellar X-ray activity. Moreover, the study of magnetic activity, especially the UV and X-ray emission, helps us refine our knowledge of the habitable zone of exoplanets (e.g., Güdel et al. 2014; Robertson et al. 2015; Gallet et al. 2017). In this paper, we use the *Chandra* data archive and the Large Sky Area Multi-Object Fiber Spectroscopic Telescope (LAMOST) database to provide a sample of stars with X-ray emission and accurate stellar parameters. In Section 2, we introduce the sample selection and data reduction process. Section 3 presents the results and some discussions, including the X-ray activity in different stellar types, the bimodality of X-ray activity of G and K types, the relation between X-ray activity and age, the relation between X-ray and chromospheric activity, and the light-curve morphology of flares.

2. SAMPLE SELECTION AND DATA REDUCTION

2.1. Sample Selection

To estimate the $R_X (= L_X/L_{\text{bol}})$ of different stellar types, we first cross-matched the *Chandra* point source catalog (Wang et al. 2016b) and the LAMOST database (DR4), using a radius of $3''$. This led to 2638 unique *Chandra* sources with 3502 LAMOST spectral observations. To calculate the likelihood of mismatch, we shifted the positions of *Chandra* sources by $1'$, and cross-matched them with the LAMOST catalog again using the same radius. In this case, we obtained 76 matches, and we conclude the likelihood of mismatch is about 2.88%.

In order to have a reliable estimation of stellar parameters, we only used spectra with signal-to-noise ratio (SNR) higher than 7 in the r band. There are four kinds of classes in the LAMOST database, including “STAR”, “GALAXY”, “QSO”, and “Unknown”, and we excluded those objects with the latter three classifications. In addition, some objects classified as “STAR” are actually globular clusters or galaxies. To exclude them, we cross-matched the sample sources with SIMBAD database⁷ and checked the spectra by eye. Young stellar objects were also excluded following SIMBAD classification (e.g., young stellar object, pre-main sequence star, Orion type, T Tau star, Herbig-Haro Object, and Herbig Ae/Be star). In summary, up to 2023 LAMOST observations were excluded, including 582 observations with low SNR, 311 observations classified as “Unknown”, 41 observations of 31 globular clusters, 757 observations of 648 galaxies and QSOs, 254 observations of 179 young stellar objects, 71 observations of 31 binaries, and seven observations of four other sources (one planetary nebula, two white dwarfs, and one cataclysmic variable). This led to 1086 unique X-ray sources with 1479 spectral observations.

2.2. Chandra Data Analysis

The subarcsecond spatial resolution of *Chandra* allows X-ray sources to be matched unambiguously to

multiwavelength counterparts. Our primary database is the *Chandra* point source catalog (Wang et al. 2016b), which includes 363,530 source detections, belonging to 217,828 distinct X-ray sources. To determine the photon counts of the sample sources, firstly we used *wavdetect* to construct the 3σ elliptical source region for each detection, by fitting a 2D elliptical Gaussian to the distribution of (observed) counts in the source cell. The broad band count rate (0.5–7 keV) and flux were then extracted with *srcflux*, which determines the net count rate (NET_RATE_APER) and model-independent flux (NET_FLUX_APER) given source and background regions. We defined the background region as an elliptical annulus around the source region, with the inner/outer radii as $2/4$ times the radii of the source ellipse.

Some sources in our sample were observed more than once by *Chandra*. In some cases, a source was detected by *wavdetect* in one observation but not detected in another observation. We calculate an upper limit using the 4σ detection threshold, which is a function of the off-axis angle and the background level (see Wang et al. 2016a, for details).

2.3. LAMOST Data

The LAMOST (also called the Guo Shou Jing Telescope) is a reflecting Schmidt telescope with an effective aperture of 4 m and a field of view of 5 degrees (Cui et al. 2012; Zhao et al. 2012). Four thousand fibres are configured on the focal surface, which enables the observation of up to 4000 objects simultaneously. The spectral resolution is $R \sim 1800$ over the wavelength range of 3690–9100 Å. After a five-year regular survey⁸ started in 2012, more than eight million spectra have been obtained. Stellar parameters, including effective temperature, surface gravity, metallicity, radial velocity, distance, and reddening, have been estimated by several studies (e.g., Wu et al. 2011; Wang et al. 2016; Xiang et al. 2017b). Such parameters can be used in many fields and may eventually revolutionize our knowledge of stellar evolution and the structure of the Milky Way. In this paper, we used the spectra from the DR4 database.

2.4. Photometric Data

We first collected the V -band magnitude from the UCAC4 catalog (Zacharias et al. 2013). For objects without a UCAC4 V -band magnitude, we calculated it using the g and r magnitudes from Pan-STARRS (Flewelling et al. 2016), following Jester et al. (2005):

$$V = g - 0.59 \times (g - r) - 0.01. \quad (1)$$

There is a small systematic offset (~ 0.1 mag) between the V magnitudes of UCAC4 and Pan-STARRS, estimated using common objects in the sample (Figure 1).

In summary, there are 484 X-ray sources with complete stellar parameters (i.e., V mag, reddening $E(B - V)$, effective temperature T_{eff} , surface gravity $\log g$, and distance). We listed X-ray properties in each *Chandra* observation for the sample sources in Table 1. We also listed LAMOST parameters for the sample stars in Table 2, including the subclass classification from Luo et al. (2015); the T_{eff} , $\log g$, $E(B - V)$, $[\text{Fe}/\text{H}]$, $[\alpha/\text{Fe}]$, and distance from Xiang et al. (2017b); the age and mass from

⁷ <http://simbad.u-strasbg.fr/simbad/>

⁸ <http://www.lamost.org/public/node/311?locale=en>

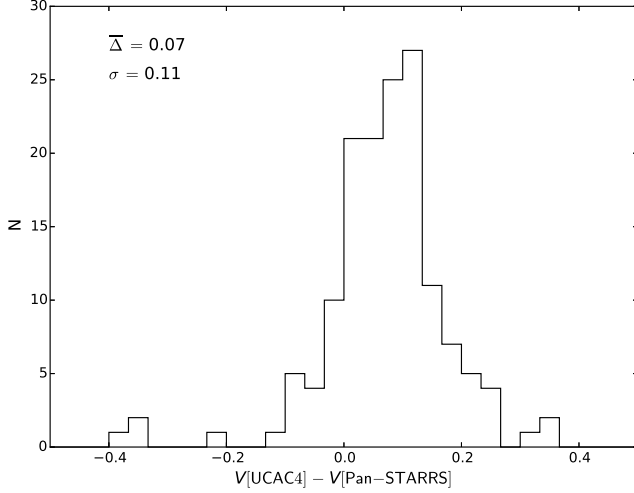


Figure 1. Comparison of V magnitudes from UCAC4 and Pan-STARRS for common objects in the sample.

Xiang et al. (2017a). Figure 2 shows the sky distribution of the sample sources in Galactic coordinates.

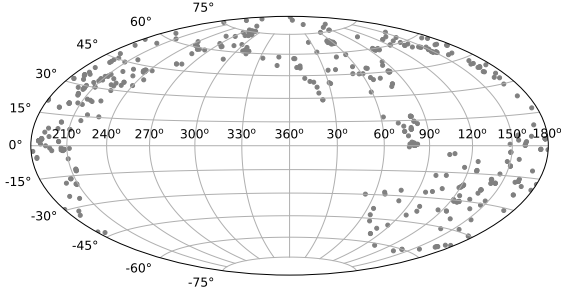


Figure 2. Sky distribution of the sample sources in this paper, in Galactic coordinates.

3. RESULTS AND DISCUSSION

In this paper, we used the ratio of X-ray to bolometric luminosities, R_X , as the X-ray activity indicator. In the X-ray band, first, we calculated an exposure-weighted averaged X-ray flux for each star. Then, we converted it to the 0.3–8 keV band using PIMMS⁹ with an APEC model (coronal temperature $\log T = 6.5$; Schmitt et al. 1990). The hydrogen column density (N_H) was converted from individual optical extinction:

$$N_H(\text{cm}^{-2}) = 2.19 \times 10^{21} A_V(\text{mag}) \quad (2)$$

(Zhu et al. 2017). The X-ray luminosity (L_X) was determined from the unabsorbed flux (f_X) and distance. The bolometric magnitude (M_{bol}) was estimated from the apparent V -band magnitude, reddening, bolometric correction, and distance:

$$M_{\text{bol}} = V - A_V - BC_V - DM, \quad (3)$$

where $A_V = 3.1 \times E(B - V)$, BC_V were obtained from Bertone et al. (2004) for dwarfs and giants with different temperatures, and DM is the distance modulus term calculated from the distance. The bolometric luminosity (L_{bol}) was then calculated using

$$\log L_{\text{bol}} = -0.4 \times (M_{\text{bol}} - M_{\text{bol},\odot}) + \log L_{\text{bol},\odot}. \quad (4)$$

The bolometric magnitude and luminosity for the Sun is 4.74 mag and $3.84 \times 10^{33} \text{ erg s}^{-1}$ (Carroll & Ostlie 1996). Finally, the R_X was calculated for the sample stars.

We should note that the unabsorbed X-ray flux, converted from the absorbed X-ray flux using PIMMS, is dependent on the coronal temperature set in the APEC model. To evaluate the influence on the R_X , we re-estimated the unabsorbed X-ray flux with a higher temperature ($\log T = 7$). Using the median value of N_H ($5.2 \times 10^{20} \text{ cm}^{-2}$) for the sample stars, the unabsorbed X-ray flux f_X decreases by $\sim 28\%$. This will lead to a decrease of $\log R_X$ by ~ 0.14 . The variation of R_X would not affect the following analysis too much.

We also calculated the X-ray hardness ratio, $HR = (c2 - c1)/(c1 + c2)$, where $c1$ is the counts of the soft band (0.3–1 keV) and $c2$ is the counts of the hard band (1–8 keV). These parameters are listed in Table 3.

3.1. X-ray Activity in Different Stellar Types

Figure 3 displays the distributions of L_X and R_X for stars from spectral type A through M. Most M type stars in LAMOST have poorly constrained values of $\log g$ and distance. Therefore, only few M type stars were included in our sample.

The L_X distribution of late-type stars (G-type or later) extends to significantly lower luminosities than early-type stars. The F, G, and K stars show a fairly wide range of emission levels, with X-ray luminosity ranging from 10^{27} to $10^{33} \text{ ergs s}^{-1}$. In these types, giants are clearly X-ray brighter than dwarfs. The F, G, and K giants are the brightest X-ray sources in our sample.

In general, late-type stars have more active ones (higher R_X) than early-type stars. Considering the similarity with solar emission, such as thermal emission-line X-ray spectrum and flares, it was suggested that X-ray emission from late-type stars originates from stellar coronae that are similar to the Sun, although sometimes much more active (Peres et al. 2000). The R_X values exhibit a wide range for stars with similar effective temperatures and surface gravities (also see Figure 4). This may represent an intrinsic range of stellar activity, although it may suffer from some uncertain factors, e.g., solar-like cyclic behaviour due to dynamos (Baliunas et al. 1995; Oláh & Strassmeier 2002), long-term variation of stellar activity such as the Maunder minimum phase of solar-type stars (Baliunas & Jastrow 1990; Henry et al. 1996; Saar et al. 1998; Gray et al. 2003), and variable X-ray emission (Soderblom 2010). The R_X ranges for each stellar type found in this paper are consistent with those observed by previous studies (Pizzolato et al. 2003; Mamajek & Hillenbrand 2008; Wright et al. 2011). This suggests that, as expected, the vast majority of these LAMOST spectra are *Chandra* source counterparts.

There are about twenty A-type stars showing X-ray activity. Generally, A-type stars are thought to be X-ray dark, since none of the X-ray production mechanisms operating in early- or late-type stars, i.e., strong

⁹ <http://cxc.harvard.edu/toolkit/pimms.jsp>

Table 1
X-ray information for the stars in our sample.

Object	ObsID	Detector	Exp. Time (s)	MJD	VigF	Count Rate (ks ⁻¹)	absorbed flux (10 ⁻¹⁵ erg cm ⁻² s ⁻¹)	Flag
(1)	(2)	(3)	(4)	(5)	(6)	(7)	(8)	(9)
J001208.1+503015	1864	s3	5876.3	51898	0.947	1.53 ^{+0.75} _{-1.06}	3.3 ^{+1.6} _{-2.3}	
J001313.2+000250	4829	s3	6658.7	53183	0.975	0.58 ^{+0.37} _{-0.66}	4.2 ^{+2.8} _{-4.9}	
J002756.6+261651	14012	i3	21692.2	56194	0.762	16.0 ^{+1.4} _{-3.1}	184 ⁺¹⁶ ₋₂₃	
	3249	i3	9977.0	52451	0.975	34.7 ^{+3.1} _{-0.1}	259 ⁺²³ _{-1.8}	
J003254.4+393821	12991	s2	34587.1	55738	0.636	0.18 ^{+0.1} _{-0.16}	3.2 ^{+2.7} _{-0.80}	
	9525	s3	34732.2	54739	0.841	0.27 ^{+0.13} _{-0.19}	1.61 ^{+1.11} _{-0.5}	
J003802.9+400824	2046	s2	14765.9	51853	0.579	1.36 ^{+0.53} _{-0.65}	18.8 ^{+9.0} _{-7.3}	
J003823.9+401250	2046	s2	14765.9	51853	0.67	28.5 ^{+2.3} _{-2.3}	176 ⁺¹⁴ ₋₁₄	
	2048	s3	13772.2	52093	0.513	19.6 ^{+2.0} _{-2.0}	93.5 ^{+9.4} _{-9.3}	
J003831.2+401711	2046	s3	14762.8	51853	0.994	0.8 ^{+0.33} _{-0.46}	1.59 ^{+0.66} _{-0.91}	
	2047	s3	14585.9	51974	0.974	1.02 ^{+0.38} _{-0.5}	2.9 ^{+1.1} _{-1.5}	
	2048	s3	13772.2	52093	0.924	0.35 ^{+0.21} _{-0.34}	1.01 ^{+0.61} _{-1.01}	
J004118.6+405159	2049	s2	14568.4	51853	0.564	8.6 ^{+1.3} _{-1.3}	50.4 ^{+7.6} _{-7.7}	
	2902	i0	4695.0	52614	0.798	7.3 ^{+1.9} _{-2.3}	57 ⁺¹⁵ ₋₁₈	
J004301.5+411052	10551	i2	3964.7	54840	0.805	< 2.26	< 29.5	u

Note. — The columns are: (1) object; (2) observation ID; (3) the detector on *Chandra* ACIS; (3) exposure time after deadtime correction; (4) Modified Julian Date for the beginning point of the observation; (6) vignetting factor; (7) net count rate in the 0.5–7 keV; (8) absorbed X-ray flux in the 0.5–7 keV. (9) “u” means the source is not detected in this observation, and an upper limit is estimated. (This table is available in its entirety in machine-readable and Virtual Observatory (VO) forms in the online journal. A portion is shown here for guidance regarding its form and content.)

Table 2
LAMOST information for the stars in our sample.

Object	Subclass	T_{eff} (K)	$\log g$	E(B-V)	[Fe/H]	[α /Fe]	Distance (pc)	Age (Gyr)	Mass (M_{\odot})
(1)	(2)	(3)	(4)	(5)	(6)	(7)	(8)	(9)	(10)
J001208.1+503015	G2	6010±61	4.56±0.11	0.07	-0.07±0.06	0.04±0.1	265±26
J001313.2+000250	F6	6340±117	4.3±0.22	0.09	0.08±0.17	0.15±0.14	641±218
J002756.6+261651	G9	5388±146	4.33±0.11	0.04	-0.05±0.08	0.12±0.1	147±13
J003254.4+393821	K1	5446±211	4.41±0.11	0.08	0.31±0.11	...	723±127
J003802.9+400824	G2	5871±60	4.61±0.11	0.05	0.02±0.06	0.06±0.1	272±23
J003823.9+401250	F9	5729±60	3.38±0.09	0.06	-0.04±0.1	0.04±0.1	1286±138
J003831.2+401711	G8	5259±121	4.03±0.18	0.1	-0.01±0.14	0.03±0.11	1337±364
J004118.6+405159	G3	5732±68	4.36±0.11	0.11	-0.13±0.09	0.04±0.1	506±87	12.0±2.9	0.91±0.06

(This table is available in its entirety in machine-readable and Virtual Observatory (VO) forms in the online journal. A portion is shown here for guidance regarding its form and content.)

Table 3
Key results for the stars in our sample.

Object	V (mag)	M_{bol} (mag)	unabsorbed f_X (10 ⁻¹⁵ erg cm ⁻² s ⁻¹)	L_X (erg s ⁻¹)	$\log R_X$	HR	Flag
(1)	(2)	(3)	(4)	(5)	(6)	(7)	(8)
J001208.1+503015	11.71±0.09	4.57	6.2±3.5	5.2e+28±3.2e+28	-4.94±0.27	-0.43±0.53	u
J001313.2+000250	12.48±0.11	3.46	8.2±7.2	4.0e+29±4.5e+29	-4.49±0.48	-0.52±0.99	u
J002756.6+261651	11.62±0.1	5.63	350±32	9.0e+29±1.8e+29	-3.27±0.10	0.1±0.04	u
J003254.4+393821	14.55±0.1	5.10	4.5±2.2	2.8e+29±1.7e+29	-3.99±0.27	0.72±0.34	u
J003802.9+400824	12.21±0.11	4.98	33±14	2.9e+29±1.3e+29	-4.03±0.20	-0.22±0.33	u
J003823.9+401250	12.3±0.11	1.71	244±22	4.8e+31±1.1e+31	-3.11±0.11	0.21±0.04	u
J003831.2+401711	15.4±0.12	4.54	3.7±1.1	8.0e+29±5.0e+29	-3.76±0.27	-0.5±0.2	u
J004118.6+405159	12.69±0.11	4.07	109±16	3.3e+30±1.2e+30	-3.33±0.17	-0.11±0.09	u

Note. — The columns are: (1) object; (2) extinction-corrected V -band magnitude; (3) bolometric magnitude; (4) unabsorbed X-ray flux in the 0.3–8 keV; (5) X-ray luminosity in the 0.3–8 keV. (6) X-ray-to-bolometric luminosity ratio; (7) Hardness ratio $HR = (c2 - c1)/(c1 + c2)$. $c1$ and $c2$ represent background-subtracted counts in soft (0.3–1 keV) and hard (1–8 keV) band, respectively. (8) “u” means V magnitude from UCAC4, while “p” means V magnitude from Pan-STARRS. (This table is available in its entirety in machine-readable and Virtual Observatory (VO) forms in the online journal. A portion is shown here for guidance regarding its form and content.)

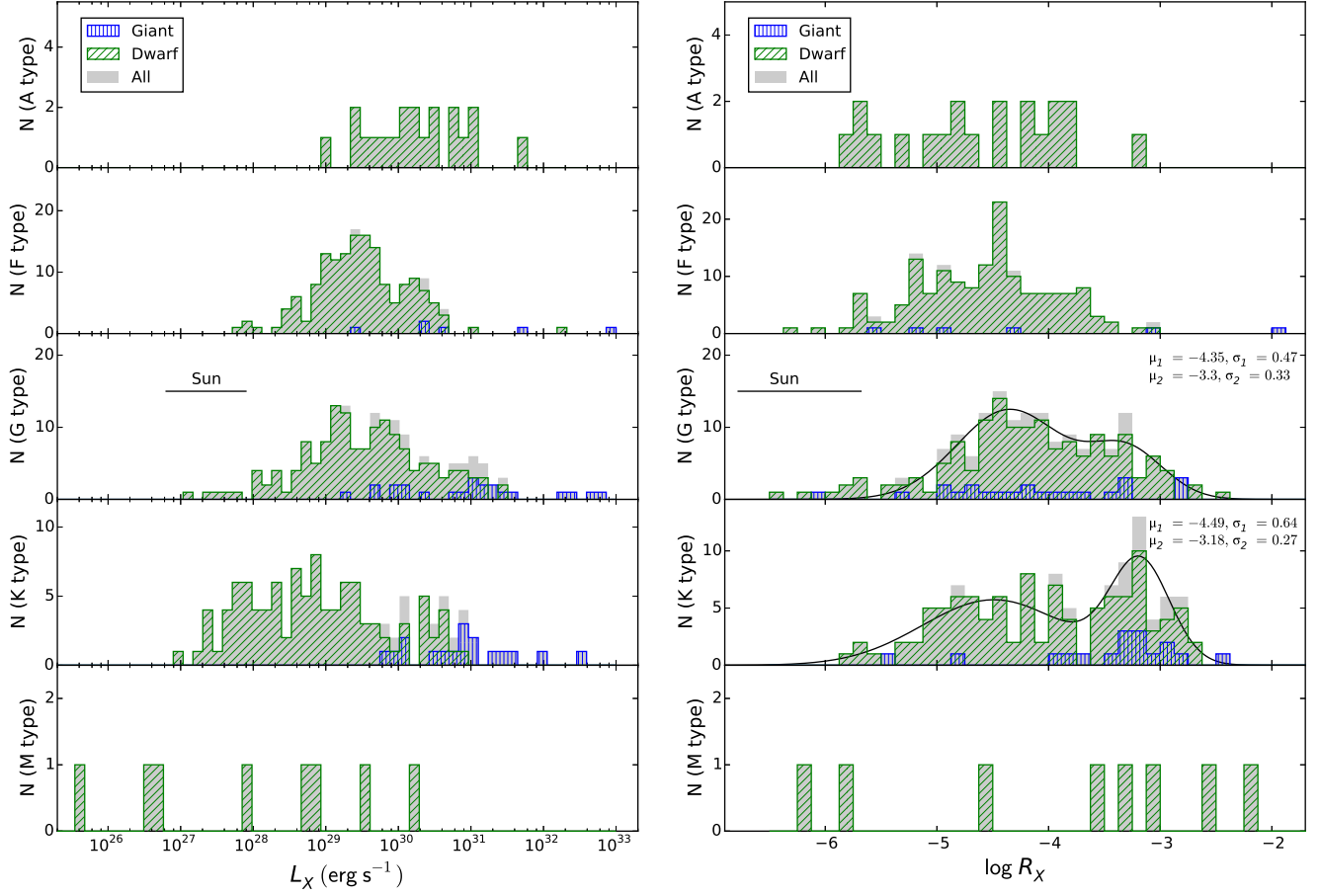


Figure 3. Left panel: Histograms showing the distributions of L_X for stars from A to M type. These histograms plotted with blue vertical lines, green slashes, and shaded area indicate giants, dwarfs, and all stars. The range of solar X-ray luminosity is $10^{26.8}$ – $10^{27.9}$ ergs s^{-1} (Judge et al. 2003), covering a typical solar cycle. Right panel: Histograms showing the distributions of R_X for stars of spectral type A through M. These histograms plotted with blue vertical lines, green slashes, and shaded area indicate giants, dwarfs, and all stars. The $\log R_X$ of the Sun varies from -6.8 to -5.7 in a typical solar cycle.

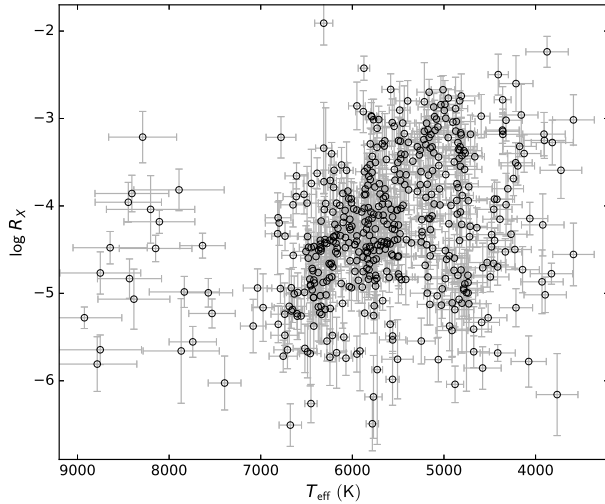


Figure 4. R_X versus T_{eff} .

winds and convection zones, ought to be valid for A-type stars. Previous studies suggested that the X-ray emitting A-types are mostly pre-main sequence (i.e., Herbig Ae/Be) stars or binaries (Zinnecker & Preibisch 1994; Pease et al. 2006; Schröder & Schmitt 2007). In the binary scenario, the X-ray emission is from an unresolved low-mass companion, often of spectral type dK or dM (Golub et al. 1983; Panzera et al. 1999). We have excluded the identified pre-main sequences and binaries (eclipsing binaries and spectral binaries) from our sample. This does not imply that the X-ray emission from the remaining A-type stars is intrinsic from the stars, because even those sources could still be unrecognized binaries.

From an inspection of the X-ray properties of our sample stars across the Hertzsprung-Russell diagram (Figure 5, left panel), we find that M dwarfs have the highest R_X but the lowest L_X values; this confirms the trend previously noted by Güdel (2004). There are 51 stars with $\log g$ smaller than 3.5, which can be classified as giants. This confirms the conclusion of previous studies (Simon & Drake 1989; Aurière et al. 2015) that late-type giants can have (high) stellar activities. Among these giants with high R_X values, some are very interesting. For example, the object J194707.6+445251 is an F5 star with the highest $\log R_X$ value (≈ -1.2) among giants. It has a radio counterpart within a $1''.5$ radius, called 4C 44.35 (Vollmer et al. 2010). The possible radio emission suggests the presence of magnetic fields and high-energy electrons (Güdel 2002). However, the high X-ray and radio emission are too high for a “normal” F-type giant. The X-ray and radio emission are possible to be a chance coincidence with one background AGN, or from the accretion process, which means the F star is in an accreting binary.

Stellar X-ray emissions are variable (Soderblom 2010), and X-ray fluxes vary for any spectral type (Figure 6). In our sample, 126 stars were observed more than once by *Chandra*. About half of them have an X-ray flux variation higher than 2. The object J131159.5-011705 has the highest flux variation (~ 36), and the variation is not due to a flare event. The flux variation would affect the correlations between R_X and other activity

indicators and stellar parameters, which may produce dissimilar results for non-simultaneous observations.

3.2. The Bimodality of X-ray Activity

The R_X distributions of G and K stars show clear bimodality (Figure 3). For G stars, there are more inactive stars than active ones, while for K stars, more active stars are apparent. We used double-gaussian functions to fit these R_X distributions: the peaks for the G type are -4.35 and -3.3 , with σ being 0.47 and 0.33 ; the peaks for the K type are -4.49 and -3.18 , with σ being 0.64 and 0.27 .

The *Chandra* data are drawn from targeted observations, which means that our sample is inhomogeneous. Therefore, it is necessary to check whether the bimodality is a result of the sampling effect, e.g., two populations of stars in different parts of the Galaxy. We divided the G- and K-type stars into two sub-samples, corresponding to stars with $\log R_X > -3.8$ and $\log R_X < -3.8$. To identify whether one source belongs to the thin disk or thick disk, we first defined one probability assuming that the velocities (U_{LSR} , V_{LSR} , W_{LSR}) follow a 3-D Gaussian distribution (Guo et al. 2016):

$$\text{Prob} = c \cdot \exp\left\{-\frac{U_{LSR}^2}{2\sigma_U^2} - \frac{(V_{LSR} - V_{\text{asym}})^2}{2\sigma_V^2} - \frac{W_{LSR}^2}{2\sigma_W^2}\right\}, \quad (5)$$

where $c = (2\pi)^{-3/2}(\sigma_U\sigma_V\sigma_W)^{-1}$ normalizes the expression. V_{asym} is the asymmetric drift, and σ_U , σ_V , and σ_W are the velocity dispersions in three dimensions, all of which varies with different components (Guo et al. 2016). Then we defined the probability ratio of belonging to the thin disk or thick disk as

$$f_{\text{thin/thick}} = \frac{\text{Prob}_{\text{thin/thick}}}{\text{Prob}_{\text{thin}} + \text{Prob}_{\text{thick}} + \text{Prob}_{\text{halo}}}. \quad (6)$$

We classified a star as being a good candidate star in the thin disk or thick disk when this ratio is larger than 80%. Figure 7 shows the classification of the sample stars in the $[\alpha/\text{Fe}]$ - $[\text{Fe}/\text{H}]$ diagram. The circles and triangles represents stars classified as in the thin disk or thick disk, using the kinematic methods. The green dashed line indicates the approximate border of thin disk and thick disk from metallicity (Masseron & Gilmore 2015). Most stars, both active and inactive, are identified as being in the thin disk. Therefore, both the metallicity and velocity information show that the bimodality is not caused by different location of the stars, i.e. the sampling effect.

Previous studies with Ca II HK, H α , and X-ray emission have found the bimodality of stellar activity, with an active and inactive peak (e.g., Stoeckel et al. 1991; Henry et al. 1996; Wright 2004; Jenkins et al. 2006, 2008, 2011; Agüeros et al. 2009; Martínez-Arnáiz et al. 2011; Pace 2013). The bimodality is explained as one saturated and one non-saturated subpopulation (Martínez-Arnáiz et al. 2011; Katsova et al. 2016), and can further be explained as one young and one old subpopulation. The latter one is often thought to be inactive in chromospheric and X-ray emission, since the magnetic activity decreases simultaneously as the rotation decelerates with age (e.g., Mamajek & Hillenbrand 2008; Katsova & Livshits 2011).

The coronal temperature is known to be positively correlated with X-ray luminosity and stellar activity (e.g.,

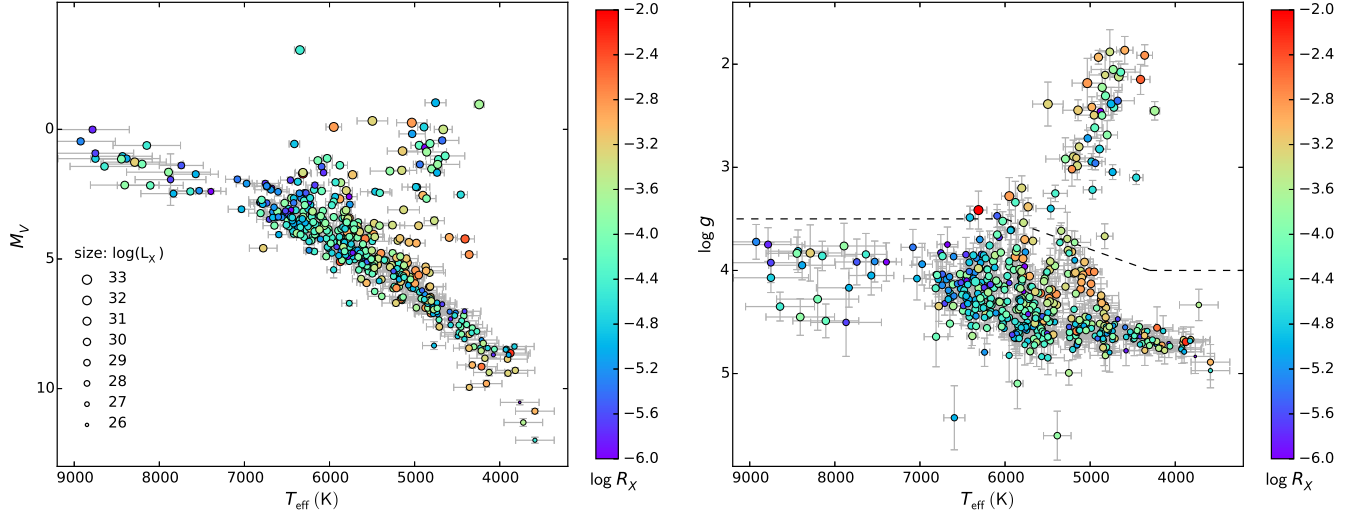


Figure 5. Left Panel: Hertzsprung-Russell diagram for the sample stars. The circle size shows the X-ray luminosity, while the color shows the X-ray to optical ratio. Right Panel: $\log g$ versus temperature for the sample sources. A star is considered to be a giant if it is above the dashed line, which is an empirical surface gravity cut separating the giant stars and dwarf stars (Ciardi et al. 2011).

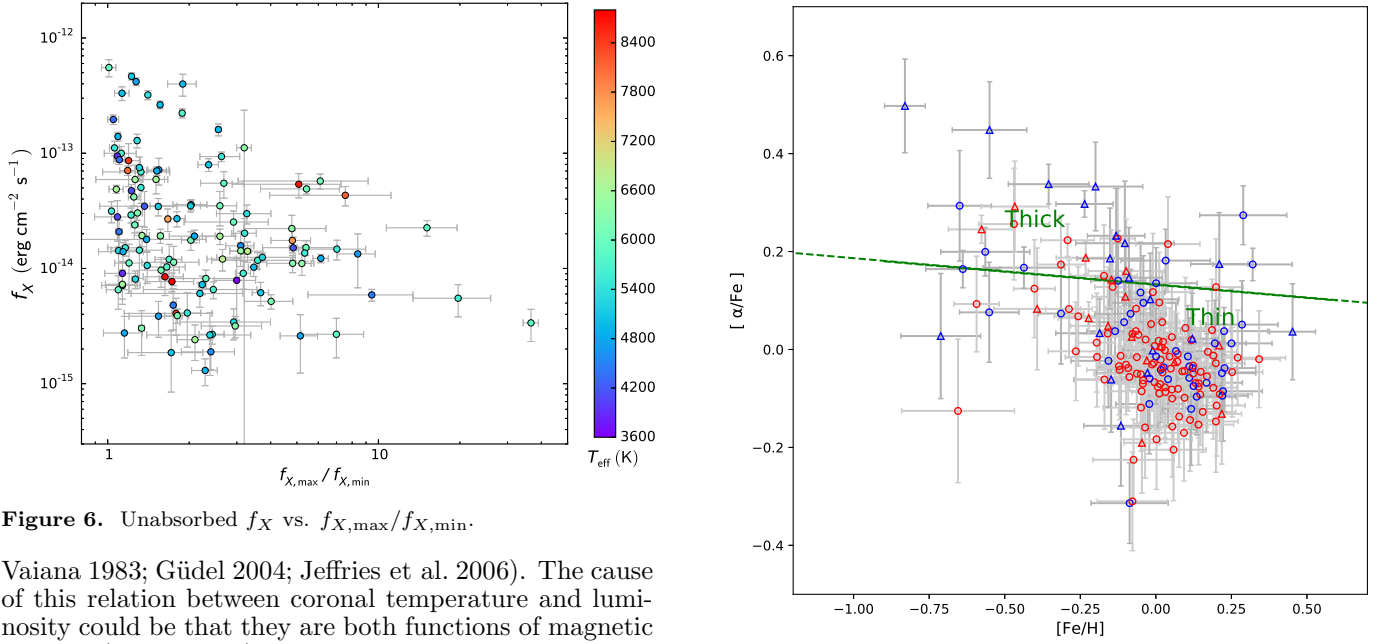


Figure 6. Unabsorbed f_X vs. $f_{X,\text{max}}/f_{X,\text{min}}$.

Vaiana 1983; Güdel 2004; Jeffries et al. 2006). The cause of this relation between coronal temperature and luminosity could be that they are both functions of magnetic activity (Güdel 2004). A more efficient dynamo inside active stars (for example because of faster rotation) produces stronger magnetic fields in the corona, and consequently a higher rate of field line reconnections and flares. This results both in a larger density of energetic electrons in the corona, and in higher temperatures. Therefore, we suggest that the double-peaked distribution of R_X represent a double-peaked distribution of heating rates, and therefore coronal temperatures. We do not have direct measurements of coronal temperatures for the stars in our sample; however, we take the X-ray hardness ratio as a proxy for the coronal temperature, because the thermal plasma emission shifts progressively to higher photon energies for higher plasma temperatures. There is a clear positive correlation between R_X and HR (Figure 8), which means stronger X-ray emitters (higher R_X) have higher coronal temperatures. *Chandra* sources are sometimes empirically classified into three groups: super-soft, quasi-soft, and hard, based on their hardness ratios

Figure 7. $[\alpha/\text{Fe}]$ versus $[\text{Fe}/\text{H}]$. The green line indicates the approximate border of thin disk and thick disk (Mason & Gilmore 2015). The circles and triangles represent stars classified as in the thin disk and thick disk, respectively, using the kinematic methods.

(Di Stefano & Kong 2003). Applying the same classification to our sample stars, we find (Figure 9) that the higher activity peak of the R_X distribution in G- and K-type stars is dominated by hard sources, and the lower activity peak by quasi-soft and super-soft sources.

3.3. The Evolution of X-ray Activity

Previous studies have shown that X-ray luminous, single, low-mass stars are the youngest (e.g., Telleschi et al. 2007), while older stars have typically lower X-ray luminosities (Flaccomio et al. 2003; Feigelson et al. 2004; Wright et al. 2010). This means that the X-ray emission decreases over the lifetime of the star. This is explained as a consequence of the stellar dynamo (e.g.,

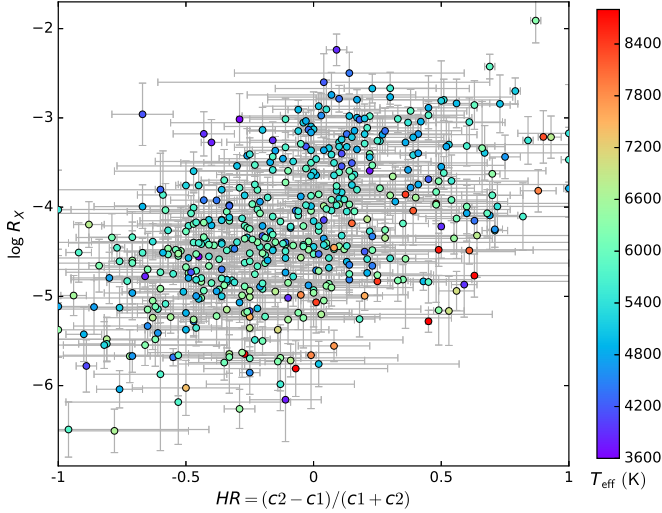


Figure 8. R_X vs. hardness ratio HR . The positive correlation means stronger X-ray emitters (higher R_X) have higher coronal temperatures.

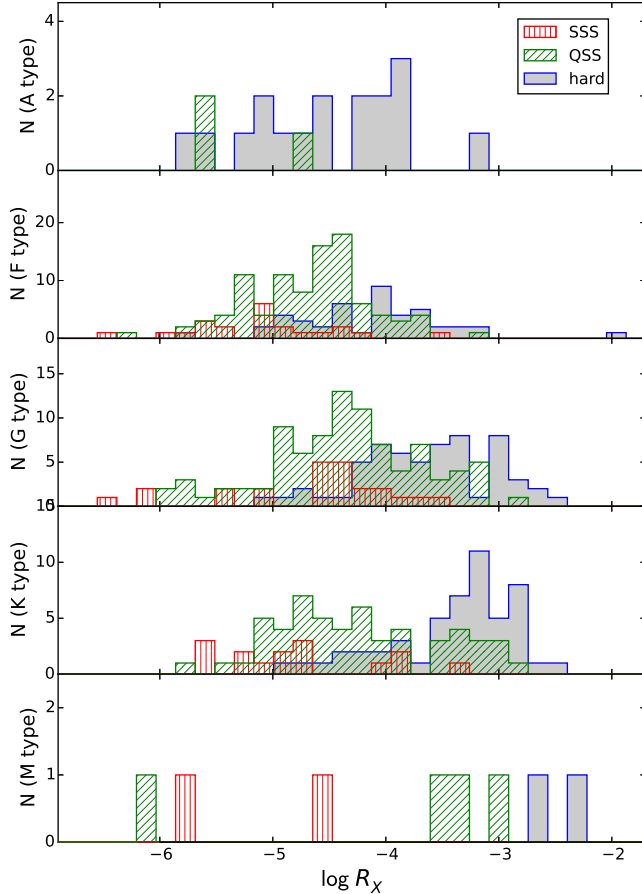


Figure 9. Histograms showing the distributions of R_X for stars from A to M type. These histograms plotted with red vertical lines, green slashes, and blue shaded area indicate SSSs, QSSs, and hard sources, respectively. Generally sources with harder X-ray spectra have higher R_X values.

Skumanich 1972; Flaccomio et al. 2003; Feigelson et al. 2004; Cranmer & Saar 2011): over time, a magnetized

stellar wind driven by the stellar dynamo leads to the loss of angular momentum and the rotational spin-down of the star, which reduces velocity shear at the tachocline between the radiative and convective zones, resulting in a reduced magnetic field (and therefore reduced activity).

Recently, many new results have been obtained about the age-activity relation. An L -shaped relation was found between the chromospheric activity (R'_{HK}) and age (Pace 2013): the chromospheric activity decreases with age for stars younger than 2 Gyr, and there is no decay of chromospheric activity after about 1.5–2 Gyr (Lyra & Porto de Mello 2005; Sissa et al. 2016). However, using SDSS observations of open clusters, Zhao et al. (2013) found that the chromospheric activity gradually declines with age, extending to at least ~ 8 Gyr. A steepening of the relation between activity and rotation was reported for stars with ages between 1 and 10 Gyr, but was possibly attributed to a non-representative sample of a few target objects. Several improved age-activity relations extending to old late-type stars have also been obtained (Mamajek & Hillenbrand 2008; Žerjal et al. 2017).

Xiang et al. (2017a) estimated ages and masses for 0.93 million main-sequence turnoff and subgiant stars, by matching with stellar isochrones employing a Bayesian algorithm, using effective temperatures, absolute magnitudes, metallicities ($[Fe/H]$), and α -element to iron abundance ratios ($[\alpha/Fe]$) deduced from the LAMOST spectra. There are 16 A types, 60 F types, and 34 G types with estimated ages and masses in our sample. We do not find a clear trend between R_X and age (Figure 10). A trough with the lowest R_X values around 2 Gyr is consistent with Pace (2013), but the reason is not clear. There are so few sources younger than 1 Gyr that we cannot confirm whether the activity keep decreasing over the first several hundred Myrs. There is also no clear trend between HR and age.

3.4. Relation Between X-ray and Chromospheric Activity

The X-ray emission and other activity indicators are proxies of stellar magnetic activity (Testa et al. 2015). The X-ray activity shows a good correlation with the activity indicators of chromosphere and transition region, e.g., Ca II HK emission (Vaiana 1983; Schrijver et al. 1992; Sterzik & Schmitt 1997), Mg II emission of dMe stars (Mathioudakis & Doyle 1989), and H α and UV emission of M dwarfs (Martínez-Arnáiz et al. 2011; Stelzer et al. 2012, 2013). LAMOST provides us with a good opportunity to study the relation between X-ray activity and H α emission.

First, we calculated the equivalent widths (EWs) of the H α emission line. The EW was calculated using the following formula:

$$EW = \int \frac{f(\lambda) - f(0)}{f(0)} d\lambda, \quad (7)$$

where $f(0)$ denotes the nearby pseudo-continuum flux. In order to trace pure chromospheric emission, we calculated the excess EW (hereafter EW') by subtracting a “basal line” of chromospheric emissions (Fang et al. 2018), which is constructed using those stars with H α absorption lines ($EW < 0$). Then, we used the CK04 stellar

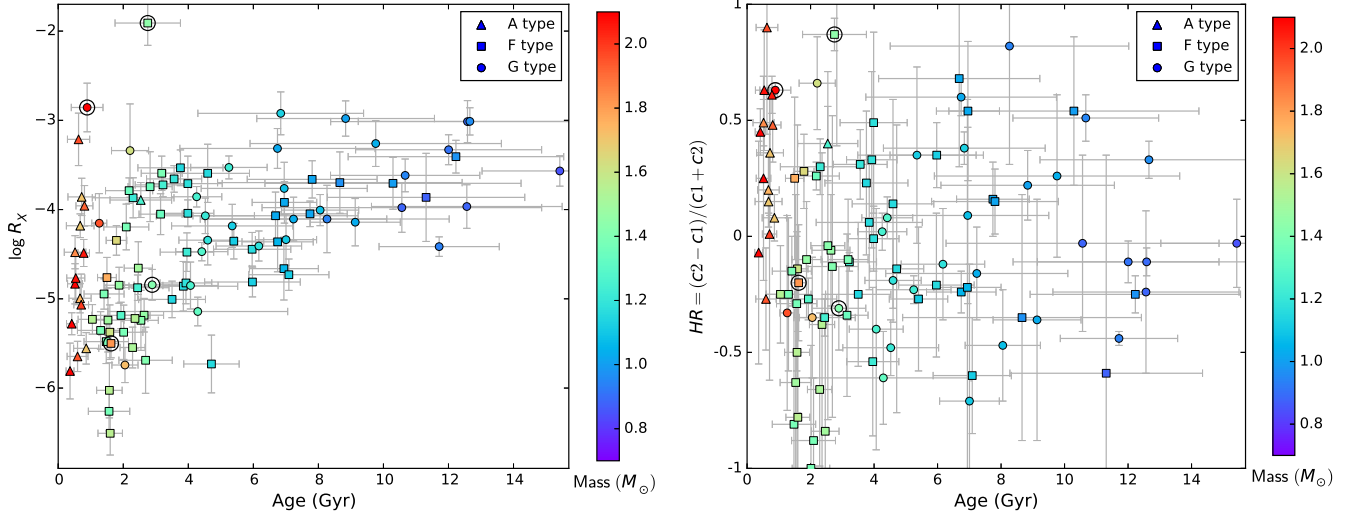


Figure 10. Left Panel: R_X vs. stellar age. A trough with lowest R_X values around 2 Gyr seems to be consistent with Pace (2013). However, no trend can be confirmed due to the uncertainty of the ages. The A, F, and G types are plotted with triangles, squares, and circles, respectively. The four objects plotted with larger black circles are giants. Right Panel: HR as a function of stellar age.

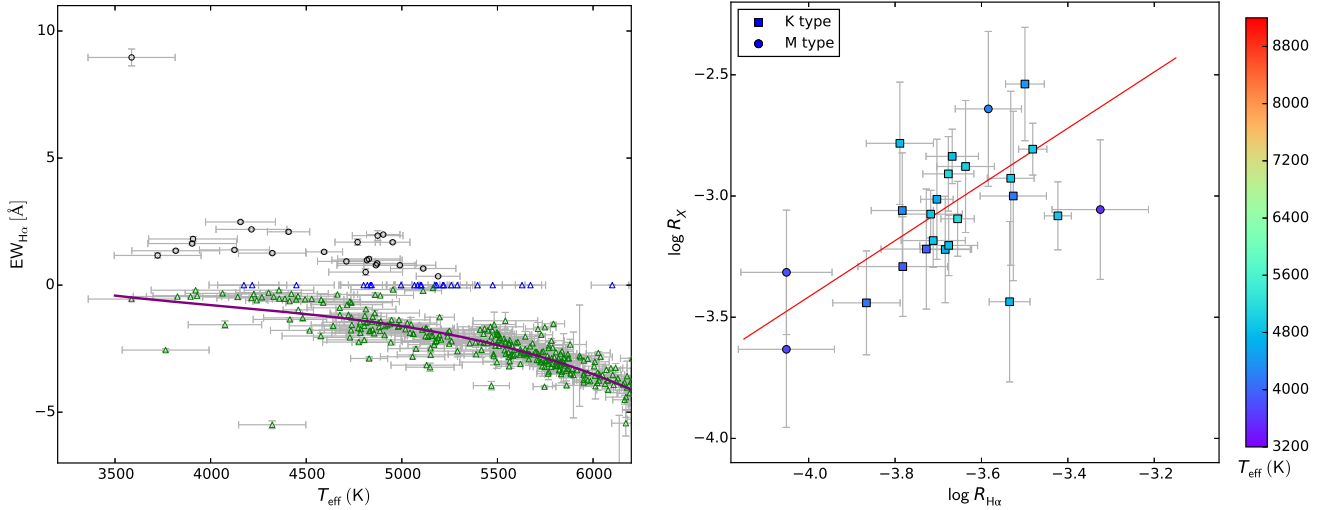


Figure 11. Left Panel: $EW_{H\alpha}$ as a function of T_{eff} . The black circles, blue triangles, green triangles represent EW values as positive, zero, and negative, respectively. The solid line is the fitted “basal line” using the stars ($3500 \text{ K} < T_{\text{eff}} < 6200 \text{ K}$) with negative EW s. Right Panel: Relation between R_X and normalized $H\alpha$ luminosity. The K and M types are plotted with squares and circles, respectively. The red line is a linear fitting to the data as $\log R_X = (1.16 \pm 0.28) \times \log R_{H\alpha} + (1.22 \pm 1.03)$.

atmosphere models (Castelli & Kurucz 2004) to transform the EW ’s to stellar surface fluxes of $H\alpha$ emission lines, $f_{H\alpha, \text{sur}}$ (Yang et al. 2017). For each star, the model with the most similar T_{eff} , $\log g$, and $[\text{Fe}/\text{H}]$ was used. Finally, we determined the flux ratio $f_{H\alpha, \text{sur}}/f_{\text{bol}, \text{sur}}$ using $f_{\text{bol}, \text{sur}} = \sigma T^4$, and calculated the $H\alpha$ emission index, $R_{H\alpha} = L_{H\alpha}/L_{\text{bol}} = f_{H\alpha, \text{sur}}/f_{\text{bol}, \text{sur}}$, to quantify stellar chromospheric activity (Table 4).

Figure 11 shows a general power law dependence of R_X on $R_{H\alpha}$:

$$\log R_X = (1.16 \pm 0.28) \times \log R_{H\alpha} + (1.22 \pm 1.03). \quad (8)$$

There are 20 K-type and 4 M-type stars in the R_X – $R_{H\alpha}$ diagram. We propose the scatter in the relations is caused by the non-simultaneous X-ray and $H\alpha$ observations. However, Stelzer et al. (2013) reported that the scatter may represent an intrinsic range of physical conditions between the corona and chromosphere. It was re-

ported by Martínez-Arnáiz et al. (2011) that in a sample of late-type dwarf active stars with spectral types from F to M, $F_X \propto F_{H\alpha}^{1.48 \pm 0.07}$. For M dwarfs, Stelzer et al. (2013) derived $R_X \propto R_{H\alpha}^{1.90 \pm 0.31}$. In this paper, we have obtained that $R_X \propto R_{H\alpha}^{1.12 \pm 0.30}$, a slightly flatter relation than found in those other studies. The discrepancy may be due to our small sample size. In addition, we are aware that the lack of simultaneous observations of those two intrinsically varying properties (coronal and chromospheric activities) introduces another source of uncertainty in all these studies (Martínez-Arnáiz et al. 2011).

3.5. Stars with X-ray Flares

Flares are in the center of the debate on the origin of coronal heating (Audard et al. 2000), with evidence showing that (X-ray or U -band) flares can release a sufficient amount of energy to produce quiescent

Table 4
Stars with H α emission lines in our sample.

Object	EW _{Hα} Å	EW' _{Hα} Å	log $R_{H\alpha}$
(1)	(2)	(3)	(4)
J004322.0+405752	1.95 \pm 0.19	3.43	-3.5 \pm 0.05
J004458.9+330431	0.51 \pm 0.13	1.93	-3.72 \pm 0.08
J013729.6+331230	1.82 \pm 0.1	2.63	-3.64 \pm 0.1
J022641.9+002811	0.35 \pm 0.02	2.2	-3.59 \pm 0.04
J024132.9+002053	2.48 \pm 0.05	3.42	-3.48 \pm 0.08
J033102.5+434758	0.65 \pm 0.05	2.41	-3.62 \pm 0.06
J034501.5+321050	0.78 \pm 0.06	2.39	-3.58 \pm 0.07
J034631.1+240702	1.64 \pm 0.05	2.45	-3.69 \pm 0.1
J040355.6+261652	1.35 \pm 0.06	2.13	-3.93 \pm 0.11
J054143.2-020353	1.03 \pm 0.07	2.46	-3.62 \pm 0.06
J054211.2-015943	0.85 \pm 0.05	2.33	-3.66 \pm 0.07
J063005.3+054540	2.1 \pm 0.07	3.19	-3.46 \pm 0.04
J063324.2+222837	8.96 \pm 0.33	9.64	-3.29 \pm 0.11
J071618.9+374451	1.69 \pm 0.12	3.07	-3.49 \pm 0.05
J095817.1+362216	1.17 \pm 0.1	1.9	-3.89 \pm 0.11
J095948.8-051413	0.93 \pm 0.07	2.26	-3.63 \pm 0.06
J111032.9+570633	1.99 \pm 0.02	3.5	-3.39 \pm 0.03
J111637.2+013249	1.26 \pm 0.05	2.29	-3.72 \pm 0.07
J122837.2+015720	2.19 \pm 0.03	3.16	-3.54 \pm 0.08
J131156.7-011311	0.78 \pm 0.03	2.25	-3.66 \pm 0.07
J203323.0+411222	1.69 \pm 0.05	3.25	-3.44 \pm 0.03
J203552.9+411503	1.39 \pm 0.05	2.31	-3.79 \pm 0.08
J223606.9+012603	1.31 \pm 0.05	2.53	-3.65 \pm 0.04
J224506.0+394016	0.98 \pm 0.05	2.4	-3.62 \pm 0.07

coronal emission (Doyle & Butler 1985; Skumanich 1985; Pallavicini et al. 1990; Pandey & Singh 2008; Pye et al. 2015). The light curves of flares can help us understand the characteristics of the coronal structures and, therefore, of the magnetic field (Schmitt & Favata 1999; Favata et al. 2000; Reale et al. 2004; Pandey & Singh 2008).

The X-ray emission from flares is indicative of very energetic, transient phenomena, associated with energy release via magnetic reconnection (Pye et al. 2015). X-ray flares differ considerably among different stars (Benz & Güdel 2010), e.g., in shape (Cully et al. 1993; Graffagnino et al. 1995; Osten & Brown 1999), peak luminosity ($\approx 10^{26}$ – 10^{33} erg s $^{-1}$) and total energy ($\approx 10^{28}$ – 10^{37} erg) (Kuerster & Schmitt 1996; Güdel et al. 2002; Osten et al. 2007; Getman et al. 2008), and rise and decay times (Haisch et al. 1987; Tagliaferri et al. 1991; Cully et al. 1994; Benz & Güdel 2010).

We selected stars with X-ray flares by eye (Table 5). The light curves of the flares are clearly variable (Figure 12). Some flares are like compact solar flares with short duration (e.g., J122837.2+015720); some flares show quite long duration (e.g., J055207.8+322639); some flares have a low rise shape (e.g., J063324.2+222837); some flares have strong absorption (e.g., J193015.7+493209). The morphological differences indicate different processes of energy release in these flares (Pandey & Singh 2008). For example, compact flares suggest a quick energy release, while a prolonged energy release is preferred for long decay flares (Pallavicini et al. 1977, 1988).

4. CONCLUSION

The *Chandra* and LAMOST data allow us to probe stellar X-ray activity over a wide range of stellar parameters. In this paper, we cross-matched the *Chandra* point

Table 5
Stars with X-ray flares in our sample.

Object	Subclass	ObsID	Duration (s)
(1)	(2)	(3)	(4)
J004118.6+405159	G3	2049	4500
J055207.8+322639	G2	13656	43000
J063214.1+045627	A2IV	3750	>15000
J063324.2+222837	M3	4467	>20000
J122837.2+015720	M0	1712	4000
J131156.7-011311	K1	1663	4000
J151628.4+070241	K5	5807	15000
J155710.7+055321	K3	11363	>5000
J193015.7+493209	G9	13612	6000
J203323.0+411222	K0	10956	11000
J221802.3+022138	K1	2981	14000
J224506.0+394016	K4	2195	14000

source catalog (Wang et al. 2016b) and the LAMOST database (DR4), and obtained a sample of 1086 stars with X-ray emission and at least one LAMOST spectral observation. Finally, the X-ray-to-bolometric luminosity R_X was estimated for 484 sources, for which the optical magnitude and complete stellar parameters (T_{eff} , $\log g$, $E(B - V)$, distance) can be obtained. Using this sample, we carefully studied the correlation between stellar X-ray activity and stellar parameters. We are aware that our sample is not unbiased, because the X-ray data come from targeted observations. Therefore, our results must not be taken as representative of the whole Galactic stellar population, but rather as a hint for further investigations based on larger samples.

The main conclusions of this paper are summarized as follows:

(1) The R_X distributions of G and K stars show a bimodal profile. Although our sample is not inhomogeneous, it is consistent with previous studies finding bimodal stellar activity. For G stars, there are more inactive stars than active ones, while for K stars, more active stars are apparent. This bimodality represents two sub-populations with different coronal temperatures. Stars with a hotter corona — observationally with a higher hardness ratio — have a higher X-ray R_X value. Using metallicity and velocity information, we ascertain that most of those G and K stars (both the active and inactive ones) are located in the thin disk. Hence, the observed bimodality cannot be associated to different sub-populations in younger and older structures of the Galaxy.

(2) There are ≈ 51 giants showing X-ray emission, and some have high X-ray activity. This confirms previous observations of stellar activity (e.g., X-ray emission, chromospheric emission, photometric variability) among giants. However, one should note that some giants or sub-giants showing stellar activity may be unrecognized binary systems (Özdarcan & Dal 2018). Also, some A-type stars show X-ray activity. Our data are not sufficient to associate the X-ray emission to the A-type stars themselves or their unresolved low-mass companions (Schröder & Schmitt 2007). These stars may be interesting candidates for follow-up observations.

(3) We find no trend of R_X with stellar age. How-

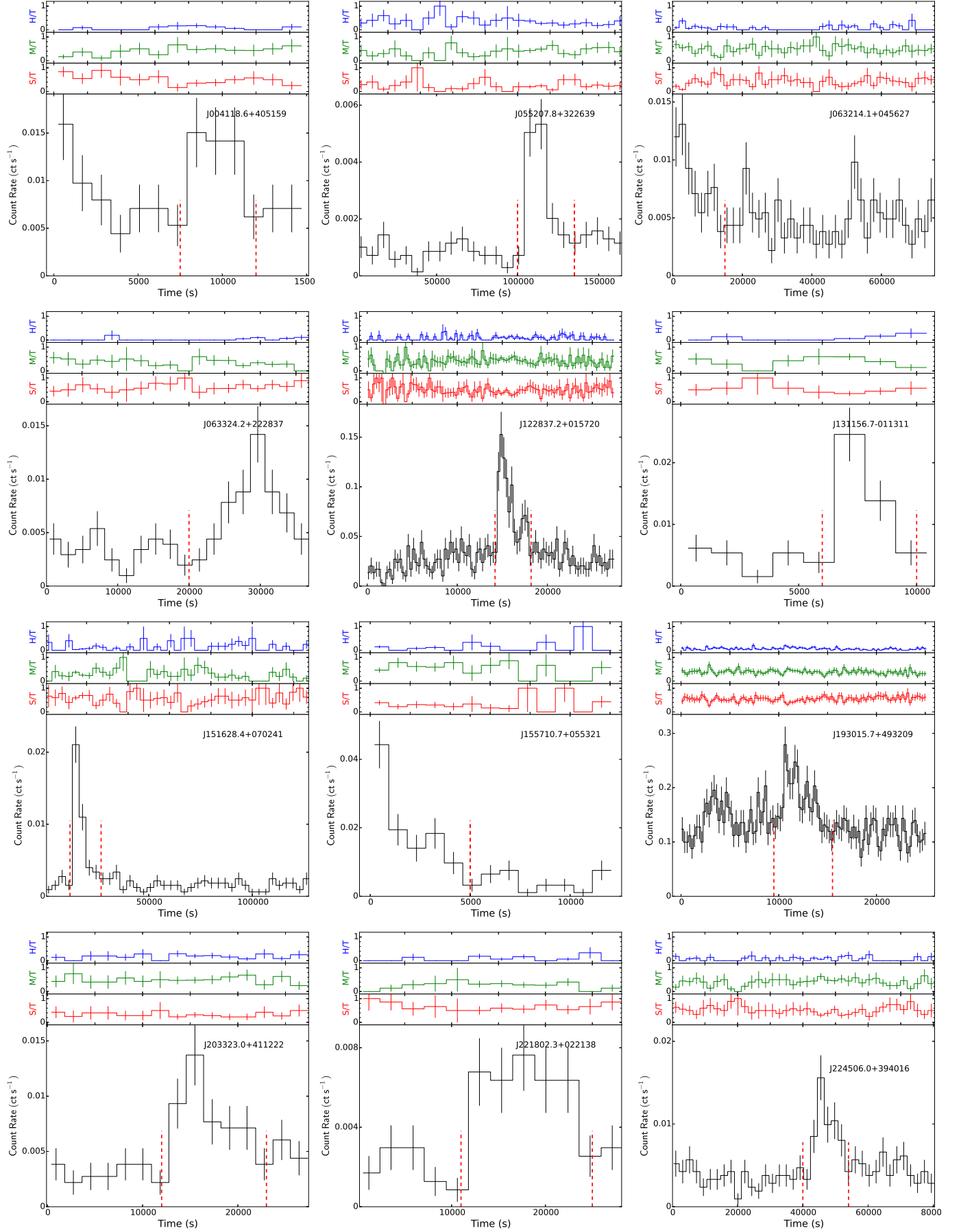


Figure 12. Stars with X-ray flares. The red dashed lines show the beginning times and/or the ending times of the flares, which are roughly determined by eyes.

ever, owing to the small sample and the uncertainty on our ages, we cannot confirm whether the activity still decreases with age after 2 Gyr or keeps constant for older stars. A trough with the lowest R_X values around 2 Gyr seems consistent with Pace (2013), but the reason for this dip is not clear.

(4) We calculated the $H\alpha$ emission index $R_{H\alpha}$ using the EWs from LAMOST spectra. The proxy of coronal activity (R_X) and the proxy of chromospheric activity ($R_{H\alpha}$) show a positive tight correlation: $\log R_X = (1.16 \pm 0.28) \times \log R_{H\alpha} + (1.22 \pm 1.03)$.

(5) We studied the light-curve morphology of the flares for twelve stars. The light curves show evident morphological differences (e.g., duration time and shape), indicating different processes of energy release, and possibly different coronal structures. We are currently planning a follow-up study to search for stellar X-ray flares using the *Chandra* archive, and investigate the flare properties in different stellar types.

We especially thank the anonymous referee for his/her thorough report and helpful comments and suggestions that have significantly improved the paper. This work has made use of data obtained from the *Chandra* Data Archive, and software provided by the *Chandra* X-ray Center (CXC) in the application packages CIAO. Guoshoujing Telescope (the Large Sky Area Multi-Object Fiber Spectroscopic Telescope LAMOST) is a National Major Scientific Project built by the Chinese Academy of Sciences. Funding for the project has been provided by the National Development and Reform Commission. LAMOST is operated and managed by the National Astronomical Observatories, Chinese Academy of Sciences. We acknowledge use of the SIMBAD database and the VizieR catalogue access tool, operated at CDS, Strasbourg, France, and of Astropy, a community-developed core Python package for Astronomy (Astropy Collaboration, 2013). We are grateful for support from the National Science Foundation of China (NSFC, Nos. 11273028, 11333004, 11603035, 11603038, and 11503054). RS acknowledges support from a Curtin University Senior Research Fellowship; he is also grateful for support, discussions and hospitality at the Strasbourg Observatory during part of this work.

REFERENCES

- Agüeros, M. A., Anderson, S. F., Covey, K. R., et al. 2009, *ApJS*, 181, 444
- Audard, M., Güdel, M., Drake, J. J., & Kashyap, V. L. 2000, *ApJ*, 541, 396
- Aurière, M., Konstantinova-Antova, R., Charbonnel, C., et al. 2015, *A&A*, 574, A90
- Baliunas, S. L., Donahue, R. A., Soon, W. H., et al. 1995, *ApJ*, 438, 269
- Baliunas, S., & Jastrow, R. 1990, *Nature*, 348, 520
- Benz, A. O., & Güdel, M. 2010, *ARA&A*, 48, 241
- Bertone, E., Buzzoni, A., Chávez, M., & Rodríguez-Merino, L. H. 2004, *AJ*, 128, 829
- Blackman, E. G., & Thomas, J. H. 2015, *MNRAS*, 446, L51
- Booth, R. S., Poppenhaeger, K., Watson, C. A., Silva Aguirre, V., & Wolk, S. J. 2017, *MNRAS*, 471, 1012
- Cardini, D., & Cassatella, A. 2007, *ApJ*, 666, 393
- Carroll, B. W., & Ostlie, D. A. 1996, *An Introduction to Modern Astrophysics* (Cambridge: Pearson)
- Castelli, F., & Kurucz, R. L. 2004, *arXiv:astro-ph/0405087*
- Charbonneau, P. 2010, *Living Reviews in Solar Physics*, 7, 3
- Ciardi, D. R., von Braun, K., Bryden, G., et al. 2011, *AJ*, 141, 108
- Cincunegui, C., Díaz, R. F., & Mauas, P. J. D. 2007, *A&A*, 469, 309
- Cranmer, S. R., & Saar, S. H. 2011, *ApJ*, 741, 54
- Cranmer, S. R., van Ballegoijen, A. A., & Edgar, R. J. 2007, *ApJS*, 171, 520
- Cui, X.-Q., Zhao, Y.-H., Chu, Y.-Q., et al. 2012, *Research in Astronomy and Astrophysics*, 12, 1197
- Cully, S. L., Fisher, G. H., Abbott, M. J., & Siegmund, O. H. W. 1994, *ApJ*, 435, 449
- Cully, S. L., Siegmund, O. H. W., Vedder, P. W., & Vallergera, J. V. 1993, *ApJL*, 414, L49
- Di Stefano, R., & Kong, A. K. H. 2003, *arXiv:astro-ph/0311374*
- Donahue, R. A. 1993, Ph.D. Thesis, New Mexico State Univ.
- Doyle, J. G., & Butler, C. J. 1985, *Nature*, 313, 378
- Fang, X.-S., Zhao, G., Zhao, J.-K., & Bharat Kumar, Y. 2018, *MNRAS*, 476, 908
- Favata, F., Micela, G., & Reale, F. 2000, *A&A*, 354, 1021
- Feigelson, E. D., Hornschemeier, A. E., Micela, G., et al. 2004, *ApJ*, 611, 1107
- Flaccomio, E., Damiani, F., Micela, G., et al. 2003, *ApJ*, 582, 398
- Flewelling, H. A., Magnier, E. A., Chambers, K. C., et al. 2016, *arXiv:1612.05243*
- Gallet, F., Charbonnel, C., Amard, L., et al. 2017, *A&A*, 597, A14
- Güdel, M. 2004, *A&A Rev.*, 12, 71
- Güdel, M. 2002, *ARA&A*, 40, 217
- Güdel, M., Audard, M., Skinner, S. L., & Horvath, M. I. 2002, *ApJL*, 580, L73
- Güdel, M., Dvorak, R., Erkaev, N., et al. 2014, *Protostars and Planets VI*, 883
- Getman, K. V., Feigelson, E. D., Micela, G., et al. 2008, *ApJ*, 688, 437-455
- Golub, L., Harnden, F. R., Jr., Maxson, C. W., et al. 1983, *ApJ*, 271, 264
- Gondoin, P. 2012, *A&A*, 546, A117
- Graffagnino, V. G., Wonnacott, D., & Schaeidt, S. 1995, *MNRAS*, 275, 129
- Gray, R. O., Corbally, C. J., Garrison, R. F., McFadden, M. T., & Robinson, P. E. 2003, *AJ*, 126, 2048
- Guo, J.-C., Liu, C., & Liu, J.-F. 2016, *Research in Astronomy and Astrophysics*, 16, 44
- Haisch, B. M., Butler, C. J., Doyle, J. G., & Rodono, M. 1987, *A&A*, 181, 96
- Henry, T. J., Soderblom, D. R., Donahue, R. A., & Baliunas, S. L. 1996, *AJ*, 111, 439
- Jeffries, R. D. 2014, *EAS Publications Series*, 65, 289
- Jeffries, R. D., Evans, P. A., Pye, J. P., & Briggs, K. R. 2006, *MNRAS*, 367, 781
- Jenkins, J. S., Jones, H. R. A., Pavlenko, Y., et al. 2008, *A&A*, 485, 571
- Jenkins, J. S., Jones, H. R. A., Tinney, C. G., et al. 2006, *MNRAS*, 372, 163
- Jenkins, J. S., Murgas, F., Rojo, P., et al. 2011, *A&A*, 531, A8
- Jester, S., Schneider, D. P., Richards, G. T., et al. 2005, *AJ*, 130, 873
- Judge, P. G., Solomon, S. C., & Ayres, T. R. 2003, *ApJ*, 593, 534
- Katsova, M. M., & Livshits, M. A. 2011, *Astronomy Reports*, 55, 1123
- Katsova, M. M., Livshits, M. A., Mishenina, T. V., & Nizamov, B. A. 2016, 19th Cambridge Workshop on Cool Stars, Stellar Systems, and the Sun (CS19), 124
- Klimchuk, J. A. 2006, *Sol. Phys.*, 234, 41
- Kraft, R. P. 1967, *ApJ*, 150, 551
- Kuerster, M., & Schmitt, J. H. M. M. 1996, *A&A*, 311, 211
- Lachaume, R., Dominik, C., Lanz, T., & Habing, H. J. 1999, *A&A*, 348, 897
- Lucy, L. B., & White, R. L. 1980, *ApJ*, 241, 300
- Luo, A.-L., Zhao, Y.-H., Zhao, G., et al. 2015, *Research in Astronomy and Astrophysics*, 15, 1095
- Lyra, W., & Porto de Mello, G. F. 2005, *A&A*, 431, 329
- Maccacaro, T., Gioia, I. M., Wolter, A., Zamorani, G., & Stocke, J. T. 1988, *ApJ*, 326, 680
- Mamajek, E. E., & Hillenbrand, L. A. 2008, *ApJ*, 687, 1264-1293
- Martínez-Arnáiz, R., López-Santiago, J., Crespo-Chacón, I., & Montes, D. 2011, *MNRAS*, 414, 2629
- Masseron, T., & Gilmore, G. 2015, *MNRAS*, 453, 1855
- Mathioudakis, M., & Doyle, J. G. 1989, *A&A*, 224, 179

- Mathur, S., Garc a, R. A., Ballot, J., et al. 2014, *A&A*, 562, A124
- Micela, G., Sciortino, S., Serio, S., et al. 1985, *ApJ*, 292, 172
- Narain, U., & Ulmschneider, P. 1990, *Space Sci. Rev.*, 54, 377
- Ol h, K., & Strassmeier, K. G. 2002, *Astronomische Nachrichten*, 323, 361
- Osten, R. A., & Brown, A. 1999, *ApJ*, 515, 746
- Osten, R. A., Drake, S., Tueller, J., et al. 2007, *ApJ*, 654, 1052
-  zdarcan, O., & Dal, H. A. 2018, *arXiv:1801.06087*
- Pace, G. 2013, *A&A*, 551, L8
- Pace, G., & Pasquini, L. 2004, *A&A*, 426, 1021
- Pallavicini, R., Golub, L., Rosner, R., et al. 1981, *ApJ*, 248, 279
- Pallavicini, R., Monsignori-Fossi, B. C., Landini, M., & Schmitt, J. H. M. M. 1988, *A&A*, 191, 109
- Pallavicini, R., Serio, S., & Vaiana, G. S. 1977, *ApJ*, 216, 108
- Pallavicini, R., Tagliaferri, G., & Stella, L. 1990, *A&A*, 228, 403
- Pandey, J. C., & Singh, K. P. 2008, *MNRAS*, 387, 1627
- Panzer, M. R., Tagliaferri, G., Pasinetti, L., & Antonello, E. 1999, *A&A*, 348, 161
- Parkin, E. R., Pittard, J. M., Hoare, M. G., Wright, N. J., & Drake, J. J. 2009, *MNRAS*, 400, 629
- Pease, D. O., Drake, J. J., & Kashyap, V. L. 2006, *ApJ*, 636, 426
- Peres, G., Orlando, S., Reale, F., Rosner, R., & Hudson, H. 2000, *ApJ*, 528, 537
- Pizzolato, N., Maggio, A., Micela, G., Sciortino, S., & Ventura, P. 2003, *A&A*, 397, 147
- Pye, J. P., Rosen, S., Fyfe, D., & Schr der, A. C. 2015, *A&A*, 581, A28
- Reale, F., G del, M., Peres, G., & Audard, M. 2004, *A&A*, 416, 733
- Reiners, A., Sch ssler, M., & Passegger, V. M. 2014, *ApJ*, 794, 144
- Robertson, P., Roy, A., & Mahadevan, S. 2015, *ApJL*, 805, L22
- Rosner, R., Golub, L., & Vaiana, G. S. 1985, *ARA&A*, 23, 413
- Saar, S. H., Butler, R. P., & Marcy, G. W. 1998, *ApJL*, 498, L153
- Schmitt, J. H. M. M., Collura, A., Sciortino, S., et al. 1990, *ApJ*, 365, 704
- Schmitt, J. H. M. M., & Favata, F. 1999, *Nature*, 401, 44
- Schmitt, J. H. M. M., Golub, L., Harnden, F. R., Jr., et al. 1985, *ApJ*, 290, 307
- Schr der, C., & Schmitt, J. H. M. M. 2007, *A&A*, 475, 677
- Schrijver, C. J., Dobson, A. K., & Radick, R. R. 1992, *A&A*, 258, 432
- Simon, T., & Drake, S. A. 1989, *ApJ*, 346, 303
- Simon, T., Herbig, G., & Boesgaard, A. M. 1985, *ApJ*, 293, 551
- Sissa, E., Gratton, R., Desidera, S., et al. 2016, *A&A*, 596, A76
- Skumanich, A. 1985, *Australian Journal of Physics*, 38, 971
- Skumanich, A. 1972, *ApJ*, 171, 565
- Soderblom, D. R. 2010, *ARA&A*, 48, 581
- Soderblom, D. R., Duncan, D. K., & Johnson, D. R. H. 1991, *ApJ*, 375, 722
- Stelzer, B., Alcal , J., Biazzo, K., et al. 2012, *A&A*, 537, A94
- Stelzer, B., Marino, A., Micela, G., L pez-Santiago, J., & Liefke, C. 2013, *MNRAS*, 431, 2063
- Sterzik, M. F., & Schmitt, J. H. M. M. 1997, *AJ*, 114, 1673
- Stocke, J. T., Liebert, J., Gioia, I. M., et al. 1983, *ApJ*, 273, 458
- Stocke, J. T., Morris, S. L., Gioia, I. M., et al. 1991, *ApJS*, 76, 813
- Tagliaferri, G., White, N. E., Doyle, J. G., et al. 1991, *A&A*, 251, 161
- Telleschi, A., G del, M., Briggs, K. R., Audard, M., & Palla, F. 2007, *A&A*, 468, 425
- Testa, P., Saar, S. H., & Drake, J. J. 2015, *Philosophical Transactions of the Royal Society of London Series A*, 373, 20140259
- Vaiana, G. S. 1983, *Solar and Stellar Magnetic Fields: Origins and Coronal Effects*, 102, 165
- Vaiana, G. S., Cassinelli, J. P., Fabbiano, G., et al. 1981, *ApJ*, 245, 163
- Vilhu, O. 1984, *A&A*, 133, 117
- Vollmer, B., Gassmann, B., Derri re, S., et al. 2010, *A&A*, 511, A53
- Wang, S., Liu, J., Qiu, Y., et al. 2016a, *ApJS*, 224, 40
- Wang, S., Qiu, Y., Liu, J., & Bregman, J. N. 2016b, *ApJ*, 829, 20
- Wang, J., Shi, J., Zhao, Y., et al. 2016, *MNRAS*, 456, 672
- Wilson, O. C. 1963, *ApJ*, 138, 832
- Wright, J. T. 2004, *AJ*, 128, 1273
- Wright, N. J., Drake, J. J., & Civano, F. 2010, *ApJ*, 725, 480
- Wright, N. J., Drake, J. J., Mamajek, E. E., & Henry, G. W. 2011, *ApJ*, 743, 48
- Wu, Y., Luo, A.-L., Li, H.-N., et al. 2011, *Research in Astronomy and Astrophysics*, 11, 924
- Xiang, M., Liu, X., Shi, J., et al. 2017a, *ApJS*, 232, 2
- Xiang, M.-S., Liu, X.-W., Yuan, H.-B., et al. 2017b, *MNRAS*, 467, 1890
- Yang, H., Liu, J., Gao, Q., et al. 2017, *ApJ*, 849, 36
- Zacharias, N., Finch, C. T., Girard, T. M., et al. 2013, *AJ*, 145, 44
-  erjal, M., Zwitter, T., Matijevi , G., et al. 2017, *ApJ*, 835, 61
- Zhao, J. K., Oswalt, T. D., Zhao, G., et al. 2013, *AJ*, 145, 140
- Zhao, G., Zhao, Y.-H., Chu, Y.-Q., Jing, Y.-P., & Deng, L.-C. 2012, *Research in Astronomy and Astrophysics*, 12, 723
- Zhu, H., Tian, W., Li, A., & Zhang, M. 2017, *MNRAS*, 471, 3494
- Zinnecker, H., & Preibisch, T. 1994, *A&A*, 292, 152